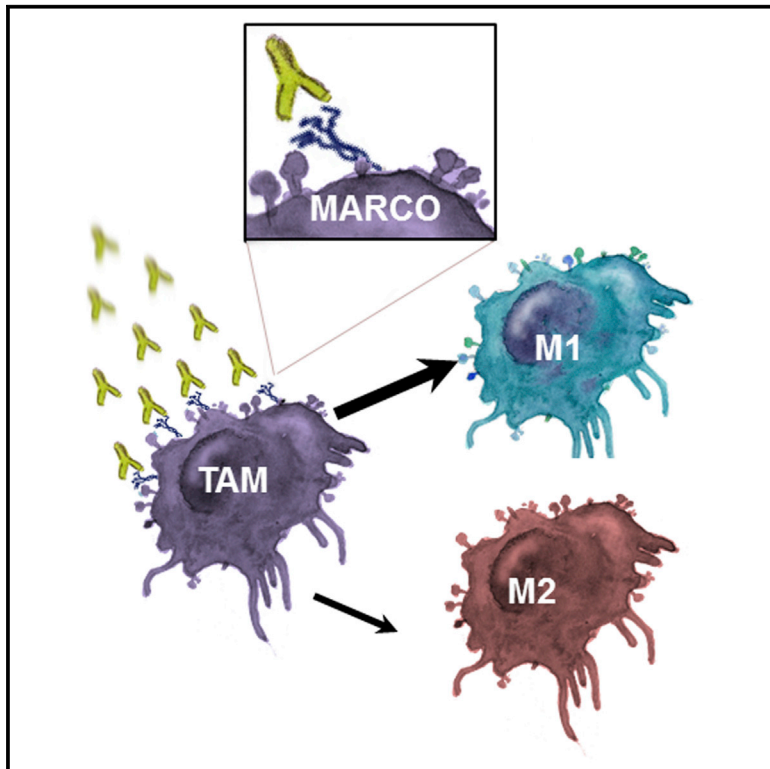


## Reprogramming Tumor-Associated Macrophages by Antibody Targeting Inhibits Cancer Progression and Metastasis

### Graphical Abstract



### Authors

Anna-Maria Georgoudaki, Kajsia E. Prokopec, Vanessa F. Boura, ..., Fubin Li, Jeffrey V. Ravetch, Mikael C.I. Karlsson

### Correspondence

mikael.karlsson@ki.se

### In Brief

Georgoudaki et al. show that tumor-associated macrophages can be targeted using an antibody toward the pattern recognition receptor MARCO. This results in altered macrophage polarization and a reduction in tumor growth and metastasis.

### Highlights

- Scavenger receptor MARCO is expressed by suppressive tumor-associated macrophages
- Antibody targeting of MARCO-expressing TAMs blocks tumor growth and metastasis
- Anti-MARCO enhances the effect of checkpoint therapy in melanoma and colon carcinoma
- MARCO is expressed on TAMs in human breast cancer and metastatic melanoma

# Reprogramming Tumor-Associated Macrophages by Antibody Targeting Inhibits Cancer Progression and Metastasis

Anna-Maria Georgoudaki,<sup>1</sup> Kajsa E. Prokopec,<sup>1</sup> Vanessa F. Boura,<sup>1</sup> Eva Hellqvist,<sup>1</sup> Silke Sohn,<sup>1</sup> Jeanette Östling,<sup>2</sup> Rony Dahan,<sup>3</sup> Robert A. Harris,<sup>4</sup> Mattias Rantalainen,<sup>5</sup> Daniel Klevebring,<sup>5</sup> Malin Sund,<sup>6</sup> Suzanne Egyhazi Brage,<sup>7</sup> Jonas Fuxe,<sup>8</sup> Charlotte Rolny,<sup>2</sup> Fubin Li,<sup>3,9</sup> Jeffrey V. Ravetch,<sup>3</sup> and Mikael C.I. Karlsson<sup>1,\*</sup>

<sup>1</sup>Department of Microbiology, Tumor and Cell Biology

<sup>2</sup>Department of Oncology and Pathology

Karolinska Institutet, 17176 Stockholm, Sweden

<sup>3</sup>Laboratory of Molecular Genetics and Immunology, The Rockefeller University, New York, NY 10065, USA

<sup>4</sup>Department of Clinical Neuroscience, Karolinska Institutet and Centre for Molecular Medicine, Karolinska University Hospital, 17176 Stockholm, Sweden

<sup>5</sup>Department of Medical Epidemiology and Biostatistics, Karolinska Institutet, 17176 Stockholm, Sweden

<sup>6</sup>Department of Surgical and Perioperative Sciences, Umeå University, 90187 Umeå, Sweden

<sup>7</sup>Department of Oncology and Pathology, Karolinska Institutet and Karolinska University Hospital, 17176 Stockholm, Sweden

<sup>8</sup>Department of Medical Biochemistry and Biophysics, Karolinska Institutet, 17176 Stockholm, Sweden

<sup>9</sup>Shanghai Institute of Immunology and Hongqiao International Institute of Medicine, Faculty of Basic Medicine, School of Medicine, Shanghai Tongren Hospital, Shanghai Jiao Tong University, and Collaborative Innovation Center of Systems Biomedicine, Shanghai 200025, China

\*Correspondence: [mikael.karlsson@ki.se](mailto:mikael.karlsson@ki.se)

<http://dx.doi.org/10.1016/j.celrep.2016.04.084>

## SUMMARY

Tumors are composed of multiple cell types besides the tumor cells themselves, including innate immune cells such as macrophages. Tumor-associated macrophages (TAMs) are a heterogeneous population of myeloid cells present in the tumor microenvironment (TME). Here, they contribute to immunosuppression, enabling the establishment and persistence of solid tumors as well as metastatic dissemination. We have found that the pattern recognition scavenger receptor MARCO defines a subtype of suppressive TAMs and is linked to clinical outcome. An anti-MARCO monoclonal antibody was developed, which induces anti-tumor activity in breast and colon carcinoma, as well as in melanoma models through reprogramming TAM populations to a pro-inflammatory phenotype and increasing tumor immunogenicity. This anti-tumor activity is dependent on the inhibitory Fc-receptor, Fc $\gamma$ RIIB, and also enhances the efficacy of checkpoint therapy. These results demonstrate that immunotherapies using antibodies designed to modify myeloid cells of the TME represent a promising mode of cancer treatment.

## INTRODUCTION

Immunotherapy is now a firmly established anti-tumor treatment approach, either alone or in combination with more-traditional treatment options such as chemotherapy (Dougan and Dranoff,

2009). Immune-modulating agents, most importantly monoclonal antibodies (mAbs), are widely used both as monotherapies and as adjuvants conditioning the tumor microenvironment (TME) for combinatorial treatments. Recent approval for the clinical use of immune checkpoint Ab therapies that enhance tumor-specific T cell immunity and restrict tumor immune tolerance offers potent ways to treat and even cure many types of cancer (Sharma and Allison, 2015). The TME is a complex structure that evolves with tumor progression to promote metastatic spread. It includes regulatory lymphocytes, but also myeloid cells, represented by different populations of macrophages known as tumor-associated macrophages (TAMs) and myeloid-derived suppressor cells (MDSCs) (Solito et al., 2014). TAMs differentiate from myeloid cells driven by cues from the growing tumor. As a reflection of the extreme plasticity of macrophages, the phenotype and composition of TAMs vary between tumor types, a number of subpopulations existing with overlapping functions (Mosser and Edwards, 2008). TAMs support tumor progression by blocking anti-tumor immunity and by secreting factors that promote angiogenesis and re-activation of epithelial-to-mesenchymal transition (EMT), which enhance metastasis (Fuxe and Karlsson, 2012). In the TME of many solid tumors, the composition of TAMs is dominated by myeloid cells with suppressive capacity (Franklin et al., 2014; Noy and Pollard, 2014). The immunosuppressive effect of TAMs stems from their enzymatic activities and production of anti-inflammatory cytokines, such as interleukin-10 (IL-10) and transforming growth factor  $\beta$  (TGF- $\beta$ ), that have an inhibitory effect on tumoricidal lymphocytes, yet augment regulatory lymphocyte populations. Selective targeting of immunosuppressive TAMs in the TME in ways that could synergize with T-cell-targeted therapies thus presents an attractive way forward. A variety of macrophage markers have been

investigated for selective expression on immunosuppressive TAMs and have been evaluated for correlation with clinical outcome (Bergamaschi et al., 2008). Recently, the “macrophage receptor with collagenous structure” (MARCO), which is a pattern-recognition receptor of the class A scavenger receptor family, was identified as a gene overexpressed in the TME and linked to poor prognosis of human breast cancer (Bergamaschi et al., 2008; Elomaa et al., 1995). However, the role of MARCO in cancer progression and the nature of the cells that express the receptor in the TME are currently unknown.

Ab-based therapies are often designed to trigger the cytotoxic activity of effector lymphocytes through the interaction of their constant region (Fc) with activating FcR on myeloid cells or NK cells, leading to Ab-dependent cellular cytotoxicity (ADCC) (Clynes et al., 2000; Taylor and Lindorfer, 2008). However, recent reports highlight the emerging use of Abs that recruit immune modulatory effector activities through the engagement of the inhibitory Fc $\gamma$ RIIb (Li and Ravetch, 2011). This highlights the importance of investigating the Fc dependence of Abs to be used in the clinic to ensure that they are effective.

Herein, we used three preclinical mouse tumor models, the 4T1 mammary carcinoma, MC38 colon cancer carcinoma, and the B16 melanoma models, to characterize the expression of MARCO in the TME and to assess its role in tumor progression. We found that MARCO expression defines a subtype of TAMs with an M2-like immunosuppressive gene signature in the TME of both mammary carcinoma and melanoma. Using anti-MARCO mAbs to target these TAMs, we induced anti-tumor activity in both the primary and metastatic breast carcinoma as well as in the primary melanoma tumor models. The anti-MARCO treatment led to alteration of the composition of TAMs in the TME into a pro-inflammatory population, thereby rendering the tumor immunogenic. We also found that anti-MARCO increases the efficacy of checkpoint therapy using anti-CTLA4 in both melanoma and colon cancer models. The anti-tumor activity was dependent on the ability of the Fc of the anti-MARCO mAbs to engage the inhibitory Fc-receptor, Fc $\gamma$ RIIB. Based on this finding and on the fact that MARCO expression is associated with a more-reactive TME signature in human breast cancer and human melanoma, these results demonstrate that immunotherapies using Abs designed to modulate myeloid cells of the TME represent a promising new mode of cancer treatment.

## RESULTS

### Identification of MARCO Expression on Immunosuppressive TAMs in the TME of Murine Mammary Carcinoma, Melanoma, and Colon Carcinoma

MARCO has a restricted expression profile on tissue-resident macrophages in the lung, lymph nodes, spleen, and peritoneum as well as on activated dendritic cells (DCs) (Matsushita et al., 2010). To investigate whether it was expressed in tumor stroma of mice, we investigated mammary carcinoma (4T1) injected in mammary fat pads as well as in melanoma (B16) and colon carcinoma (MC38) growing subcutaneously (s.c.). Using immunofluorescent staining, we found that, in the 4T1 mammary carcinoma, MARCO was co-expressed on CD11b<sup>+</sup>F4/80<sup>+</sup> TAMs (Figure 1A). Likewise, in the B16 melanoma model, MARCO<sup>+</sup>

TAMs also stained positively for both CD11b and F4/80, and in addition, MARCO<sup>+</sup> TAMs were also found in the MC38 colon carcinoma model (Figures 1B and 1C).

Importantly, MARCO was not expressed on other myeloid cells or lymphocytes including CD11c<sup>+</sup> DCs, PDCA<sup>+</sup> DCs, M1-like macrophages, TCR $\beta$ <sup>+</sup> T cells, B220<sup>+</sup> B cells, and NK1.1<sup>+</sup> natural killer (NK) cells (Figures S1A and S1B). We also verified that DCs in the tumors did not express MARCO using qPCR on sorted cells. Thus, in summary in the B16 melanoma, MARCO is only expressed by F4/80<sup>+</sup>CD11c<sup>-</sup> TAMs. Interestingly, we also found that, in the melanoma model, the MARCO-expressing TAMs were not equally distributed but were situated close to the capsule in the TME (Figure S1C). To further dissect which subtype of TAMs expressed MARCO, we sorted CD45<sup>+</sup>CD11b<sup>+</sup> TAMs from B16 tumors into four subpopulations based on their expression of Ly6C and MHCII (Movahedi et al., 2010; Figure 1D). These TAM populations represent Ly6C<sup>high</sup>MHCII<sup>low</sup> inflammatory monocytes, Ly6C<sup>high</sup>MHCII<sup>high</sup> immature macrophages, Ly6C<sup>int</sup>MHCII<sup>high</sup> classically activated (M1), and Ly6C<sup>low</sup>MHCII<sup>low</sup> alternatively activated (M2) macrophages, respectively. Using this categorization, M2 macrophages have been described to be immunosuppressive and tumor promoting in vivo, whereas M1 macrophages are inflammatory and can eradicate tumors (Noy and Pollard, 2014). Because macrophages in general are very plastic, we used qPCR to further define the TAM populations with respect to MARCO expression (Figure 1E). We found that MARCO was most highly expressed in the Ly6C<sup>low</sup>MHCII<sup>low</sup> M2-like (M2) subpopulation, which also expressed the M2 markers *cx3cr1*, *arg1*, and *retnla* (*fizz1*) but showed low expression of the M1-associated markers *h2-ab1* (*mhcl1*) and *nos2* (*inos*) (Figure 1F). Thus, MARCO is expressed by TAMs with an M2 gene signature in the TME.

### MARCO Expression Is Promoted by the Tumor and M2-Polarizing Cytokines

The expression of MARCO on immunosuppressive M2 TAMs was further supported by in vitro polarization of bone-marrow-derived macrophages (BMDMs) using tumor supernatant or cytokines. MARCO was upregulated on M2-polarized macrophages as well as on TAMs differentiated with supernatant from B16 melanoma cells (Figure 2A). These in-vitro-derived MARCO<sup>+</sup> CD68<sup>+</sup>MHCII<sup>low</sup>Ly6C<sup>-</sup>-expressing macrophages induced by tumor supernatant also co-expressed M2 markers such as CD115 and CD206 by flow cytometry as well as M2-connected genes, including cytokines *Csf1r*, *Il10*, *Arg1*, *Retnla*, and *Chi3l3*, as well as genes connected to an M2-like phenotype, *Tgfb*, *cx3cr1*, and *ccr2*, but not M1 genes (*H2-ab1*, *Nos2*, and *Il12a/b*), as determined by qPCR (Figures 2B and 2C). Considering the fact that cytokines, such as IL-10 and TGF- $\beta$ , are frequently overexpressed in the TME and can promote M2 polarization of macrophages, we studied whether these cytokines could affect MARCO expression. Indeed, we found that the expression of MARCO induced by the B16 tumor supernatant stimulation of a peritoneal macrophage cell line could be mimicked by using IL-10 or TGF- $\beta$  stimulation of M0 BMDMs (Figures S2A and S2B). Blocking experiments using Abs against IL-10 and/or TGF- $\beta$  for tumor supernatant upregulation of MARCO

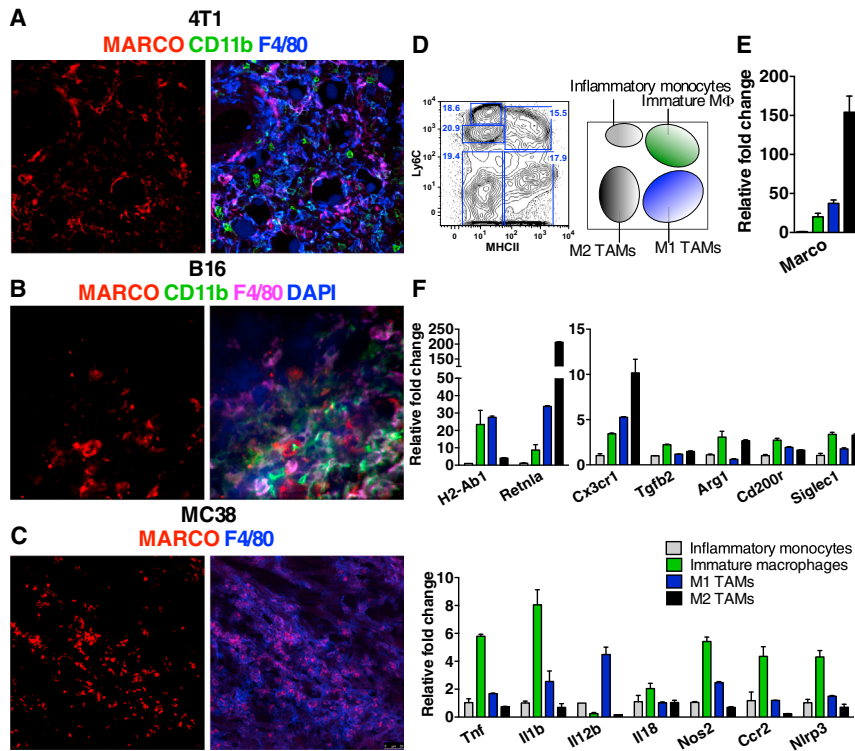


**Figure 1. Identification of MARCO as a Marker on M2 Macrophages in Tumor Stroma of Mammary Carcinoma, Melanoma, and Colon Carcinoma**

(A) Immunofluorescence (IF) staining of 4T1 mammary tumor sections. MARCO (red) as an individual channel (left) and merged (right) with CD11b (green) and F4/80 (blue) is shown.

(B) IF staining of B16 melanoma tumor sections. MARCO (red) in an individual channel (left) and merged (right) with CD11b (green), F4/80 (magenta), and DAPI (blue) is shown.

(C) IF staining of MC38 colon tumor sections. MARCO (red) in an individual channel (left) and merged (right) with F4/80 (blue) is shown. All magnifications are 63 $\times$ .

(D) Flow cytometric analysis of macrophage subpopulations sorted from B16 tumors on D10. The cells were gated on live CD45<sup>+</sup>CD11b<sup>+</sup> single cells and subsequently divided into four TAM subtypes based on Ly6C and MHCII expression; (right) Ly6C<sup>hi</sup> MHCII<sup>lo</sup> inflammatory monocytes (gray); Ly6C<sup>int</sup> MHCII<sup>hi</sup> immature macrophages (green); Ly6C<sup>lo</sup> MHCII<sup>hi</sup> M1 TAMs (blue); and Ly6C<sup>lo</sup> MHCII<sup>lo</sup> M2 TAMs (black). (Left) Graphical illustration of color-coded sorted macrophage populations, from B16 tumors, is shown.

(E) Relative expression of MARCO on sorted macrophages subpopulations from (D) normalized to inflammatory monocytes (gray).

(F) Relative expression of M1 and M2 genes by qPCR on macrophage subpopulations from (D). In (D), data show mean  $\pm$  SEM with a confidence interval (CI) of 95% of duplicates from one out of three representative experiments.

were unsuccessful (data not included), possibly due to additional factors or affected by the fact that the supernatant induced production of these cytokines by macrophages themselves (Figure 2C). These data implicate MARCO expression on TAMs in the re-activation of EMT, which is driven by TGF- $\beta$  and acts as a link between inflammation and cancer progression toward metastasis (Fuxe and Karlsson, 2012; Mani et al., 2008; Miettinen et al., 1994). Collectively, these data show that MARCO expression is driven by cytokines that are released in the TME and that it is a general marker for immunosuppressive macrophages.

### Immunotherapy Targeting MARCO Arrests Tumor Growth and Metastasis and Increases TME Immunogenicity

Based on the restricted expression pattern of MARCO on tumor-promoting TAMs, we next assessed whether MARCO could be used as a target for immunotherapy. Wild-type mice were thus injected with 4T1 cells in the mammary fat pad, and a MARCO-specific Ab was given intravenously (i.v.) followed by monitoring of tumor growth and measuring of metastasis (Figure 3A). We found that anti-MARCO immunoglobulin G (IgG) had the ability to reach MARCO-expressing TAMs in the 4T1 mammary fat pad carcinoma TME (Figure 3B). In addition, 4T1 tumor-bearing mice that were treated with anti-MARCO IgG had smaller tumors measured, as both tumor volume and weight, compared to untreated mice (Figure 3C). We also

observed that treatment with anti-MARCO IgG significantly reduced metastatic spread to the lungs as determined by *in vitro* cultures of tumor cells from the lungs of the mice (Figure 3D). Furthermore, we found that treatment with anti-MARCO IgG resulted in a shift in the composition of TAM populations in the TME of 4T1 tumors, with an increase in M1 TAMs and a concomitant decrease of the M2 TAM population (Figure 3E). To determine whether this shift rendered the tumor more immunogenic, we characterized the draining lymph nodes and observed increased germinal center formation as well as altered CD4/CD8 T cell ratio and a tendency for reduced numbers of T regulatory cells (Figures 3F and 3G).

The 4T1 mammary tumor is a potent inducer of MDSCs, which are a heterogeneous group of immature myeloid cells that suppress T cell activation and accumulate in the spleen during cancer (Sinha et al., 2007; Solito et al., 2014). We next explored the possibility that anti-MARCO treatment affected this population of cells. However, we could find no evidence for changes in either the monocytic (M-MDSC) or polymorphonuclear (PMN-MDSC) subpopulations in the spleens of tumor-bearing mice (Figure S3A). In addition, we did not observe any alterations in other lymphocyte populations including macrophages, B cells, T cells, NKT cells, or NK cells (Figures S3B–S3D). Anti-MARCO treatment therefore specifically alters TAM populations to increase immunogenicity of the tumor, and this in turn stops growth and metastatic spread to the lungs.

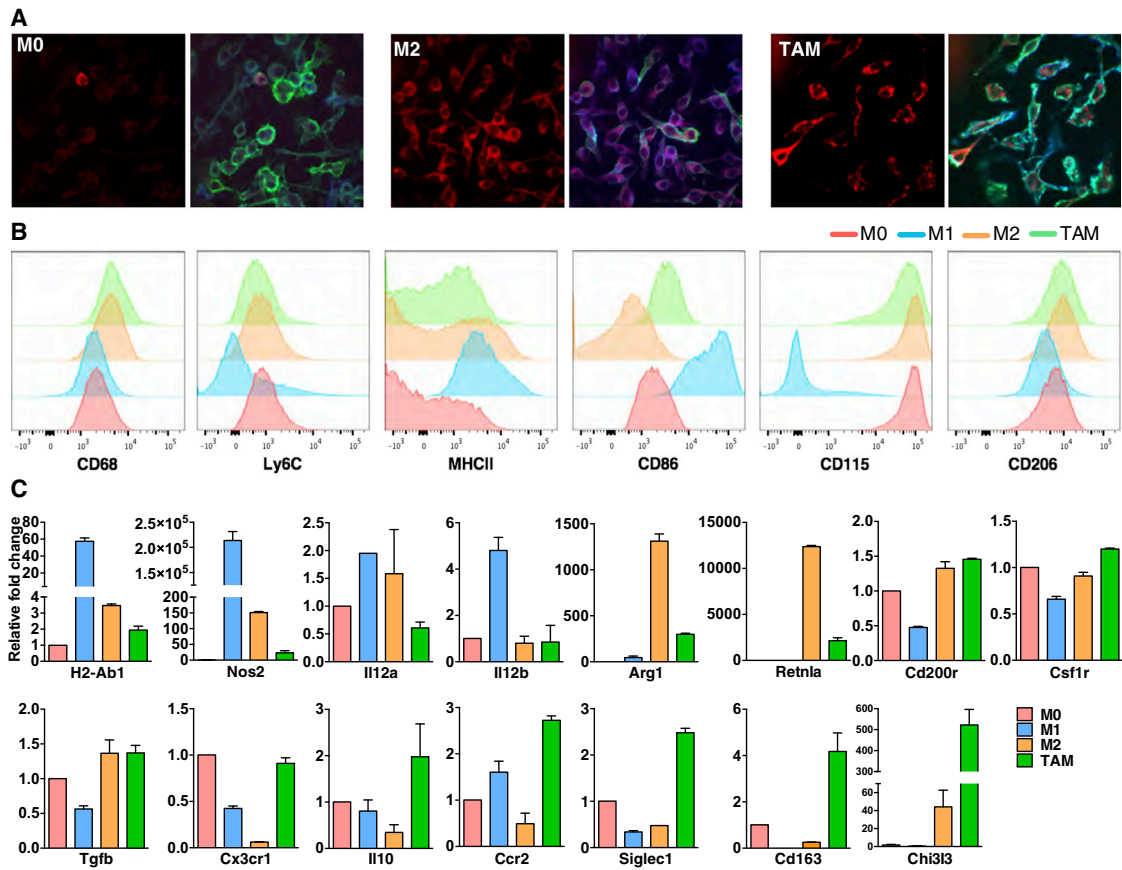


**Figure 2. Association of MARCO with M2- and Tumor-Polarizing Expression Signatures**

(A) IF stainings (63 $\times$ ) on M0, M2, and TAM (B16 tumor-supernatant)-polarized BMDMs. MARCO (red) in an individual channel (left) and merged (right) with F4/80 (blue) and CD11b (green) is shown.

(B) Flow cytometric analysis of surface marker expression on M0, M1, M2, and TAM-polarized BMDMs.

(C) Relative expression of M1 and M2 genes by qPCR on M0, M1, M2, and TAM-polarized BMDMs. In (C), data show mean  $\pm$  SEM with a CI of 95% of duplicates.

### Anti-MARCO Therapy Restricts Tumor Growth in a Melanoma Model and Promotes Immune Checkpoint Therapy

To evaluate the generality of anti-MARCO immunotherapy and to further dissect its mechanism of action, we tested its efficacy in the B16 melanoma model (Figure 4A). To create a targetable stromal compartment, B16 melanoma cells expressing luciferase were injected subcutaneously in Matrigel in the flanks of mice. These mice were subsequently treated with anti-MARCO mAbs, and tumor growth was measured using an in vivo imaging system (Figure S4A). As in the 4T1 mammary tumor model, when injected i.v. into tumor-bearing mice, the anti-MARCO Abs reached MARCO<sup>+</sup> TAMs in the stroma (Figure 4B). Likewise, the treatment significantly reduced tumor growth over the 9 days of experimental observation (Figure 4C). The TME displayed similar changes as were observed in the 4T1 model with decreased numbers of immature macrophages, an altered CD4/CD8 ratio, decreased numbers of regulatory T cells, and an increased CD4/T-reg cell ratio, whereas no effect was evident for other lymphocytes or myeloid cells (Figures S4B–S4E). When investigating gene expression of the bulk of sorted TAMs, we

found general upregulation of M1-related genes including *Ii1b* as well as a downregulation of *Ii10*, showing a shift of macrophage polarization toward M1 (Figure 4D). To directly test whether anti-MARCO treatment rendered the tumor more immunogenic, we used B16 tumors expressing membrane-bound ovalbumin (OVA). Here, we found that anti-MARCO increased the OVA-specific CD8 responses as well as increased the production of OVA-specific IgG2b (Figure S4F). Next, the efficacy of anti-MARCO treatment was compared with immunotherapies with known activity in this model and we addressed whether it could enhance ADCC or checkpoint therapy. Groups of mice were injected with anti-MARCO alone or together with an Ab against the TRP1 antigen, which induces direct ADCC of the tumor (TA99; Clynes et al., 1998; Thomson et al., 1985; Figure 4E). We found that anti-MARCO treatment had a similar effect as TA99 in arresting tumor growth, but there was no apparent additive effect when combining the two. As an important control, there was no effect of the anti-MARCO treatment on tumor growth in MARCO-deficient mice (Figure 4E). In contrast, combining anti-MARCO treatment with immune checkpoint therapy using anti-CTLA4 Abs (Leach et al., 1996) decreased

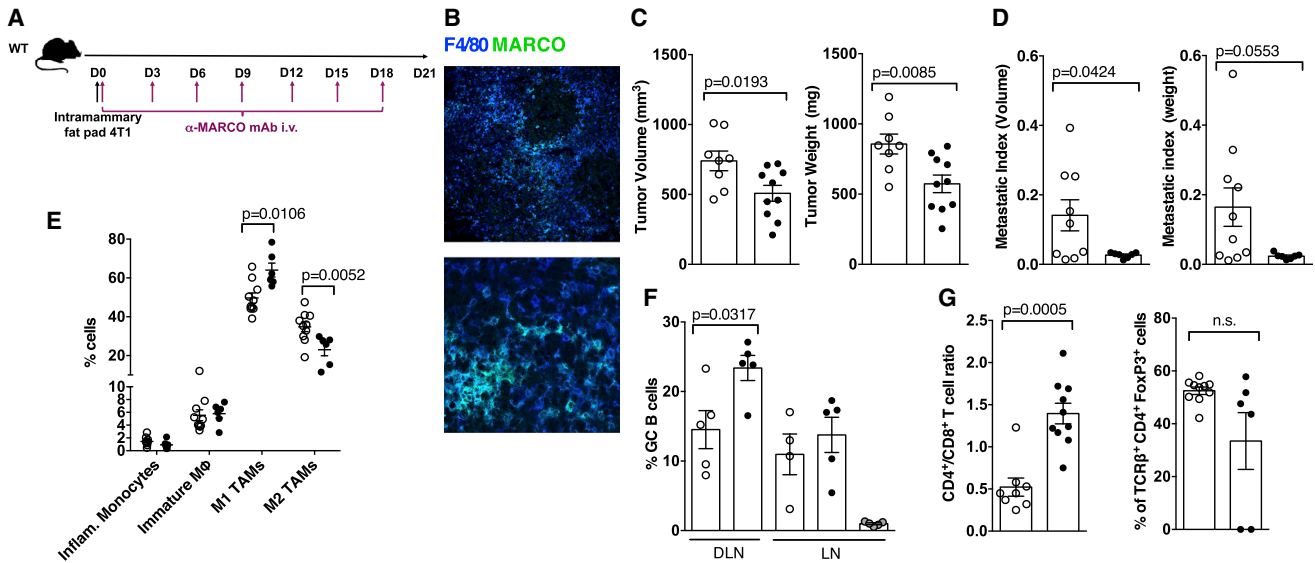


**Figure 3. Anti-MARCO Ab Treatment Inhibits Tumor Growth and Metastasis by Increasing the Immunogenicity of the Tumor Microenvironment in the 4T1 Mammary Carcinoma**

(A) Schematic of the 4T1 mammary carcinoma model and Ab treatment regimen.  
 (B) IF stainings of 4T1 mammary tumors; *in vivo* administered anti-MARCO Ab is detected in green on F4/80<sup>+</sup> (blue) macrophages in 20 $\times$  (upper panel) and 63 $\times$  (lower panel).  
 (C) 4T1 primary tumor volume (left) and weight (right) on D21.  
 (D) Metastatic index based on volume (left) and weight (right) as measured by lung tumor colony formation assay on D21.  
 (E) Percentage of 4T1 tumor-infiltrating macrophage subpopulations (same gating strategy as in Figure 1C) on D21.  
 (F) Percentage of germinal center B cells in 4T1 tumor-draining versus non-draining inguinal lymph nodes in untreated controls and anti-MARCO Ab-treated mice on D21 and naive inguinal lymph nodes from non-tumor-bearing mice.  
 (G) 4T1 tumor-infiltrating CD4<sup>+</sup>/CD8<sup>+</sup> T cell ratio on D21 (left). Frequency of tumor-infiltrating T regulatory cells on D21 (right) is shown. Untreated control (open circle), anti-MARCO Ab (filled black circle), and naive non-tumor-bearing mouse (filled gray circle) are shown.  
 Data show mean  $\pm$  SEM with a CI of 95% in one representative out of three independent experiments where n = 5–10/group.

tumor growth and also increased survival compared to CTLA-4 treatment alone (Figures 4F and 4G). This was verified in the MC38 colon carcinoma model, in which anti-MARCO Abs significantly increased the efficacy of anti-CTLA4 treatment (Figure 4H). Taken together, these data indicate that anti-MARCO treatment inhibits the growth of melanoma with a similar immune-modulatory effect as evident in mammary carcinoma. In addition, anti-MARCO enhances checkpoint therapy using anti-CTLA4 Abs in both melanoma and colon carcinoma models.

### Selective Engagement of Fc $\gamma$ R1b Is Required for the Anti-MARCO Anti-tumor Effect

Previous studies have showed that anti-tumor Abs require the engagement of distinct FcRs to either promote cytotoxicity (Clynes et al., 1998) or to induce agonistic activity through crosslinking (Li and Ravetch, 2011). To further dissect the mechanism through which engagement of anti-MARCO on TAMs resulted in alteration of the TME, we generated recombinant mouse anti-MARCO Abs with defined Fc domains that selectively engaged murine FcRs. Using these Fc variants, we determined that the Ab that was unable to bind FcRs had a diminished therapeutic effect, suggesting involvement of Fc receptors (Figure 5A). Using Fc-receptor-deficient mice lacking all Fc receptors or only activating Fc $\gamma$ RI, III, and Fc $\gamma$ RIV receptors, respectively (Smith et al., 2012; Takai et al., 1994), we found that the anti-MARCO

therapeutic effect was not dependent on activating receptors, leaving only the inhibitory Fc $\gamma$ RIIB to be responsible for the anti-tumor effect (Figure 5B). To verify the involvement of Fc $\gamma$ RIIB, we also tested the ability of anti-MARCO to decrease tumor growth in Fc $\gamma$ RIIB-deficient mice, which was less effective (Figure 5B). Supporting a macrophage-intrinsic mechanism, Fc $\gamma$ RIIB was primarily expressed on M2 TAMs as well as on *in vitro* bone-marrow-derived TAMs (Figure 5C). Fc $\gamma$ RIIB engagement is required for the agonistic activity of Abs targeting the tumor necrosis factor receptor (TNFR) superfamily members CD40 and DR5 (Li and Ravetch, 2011) by facilitating crosslinking of these trimeric receptors. It is thus likely that the anti-tumor activity of the anti-MARCO Ab also results from crosslinking of this trimeric receptor to modify TAM activation or composition.

### Expression of MARCO Correlates to M2 TAM and EMT-Metastasis-Driving Gene Signatures in Human Basal Breast Cancer and Metastatic Melanoma

To investigate the clinical relevance of an anti-MARCO treatment, we next investigated the presence of MARCO-positive TAMs by gene expression and immunohistochemistry on human primary breast cancer biopsies. Using two different human breast cancer datasets, we found that MARCO was most highly expressed in the basal (triple negative) subgroup of patients compared to LumA, LumB, and Her2<sup>+</sup> subgroups (Sørlie et al.,

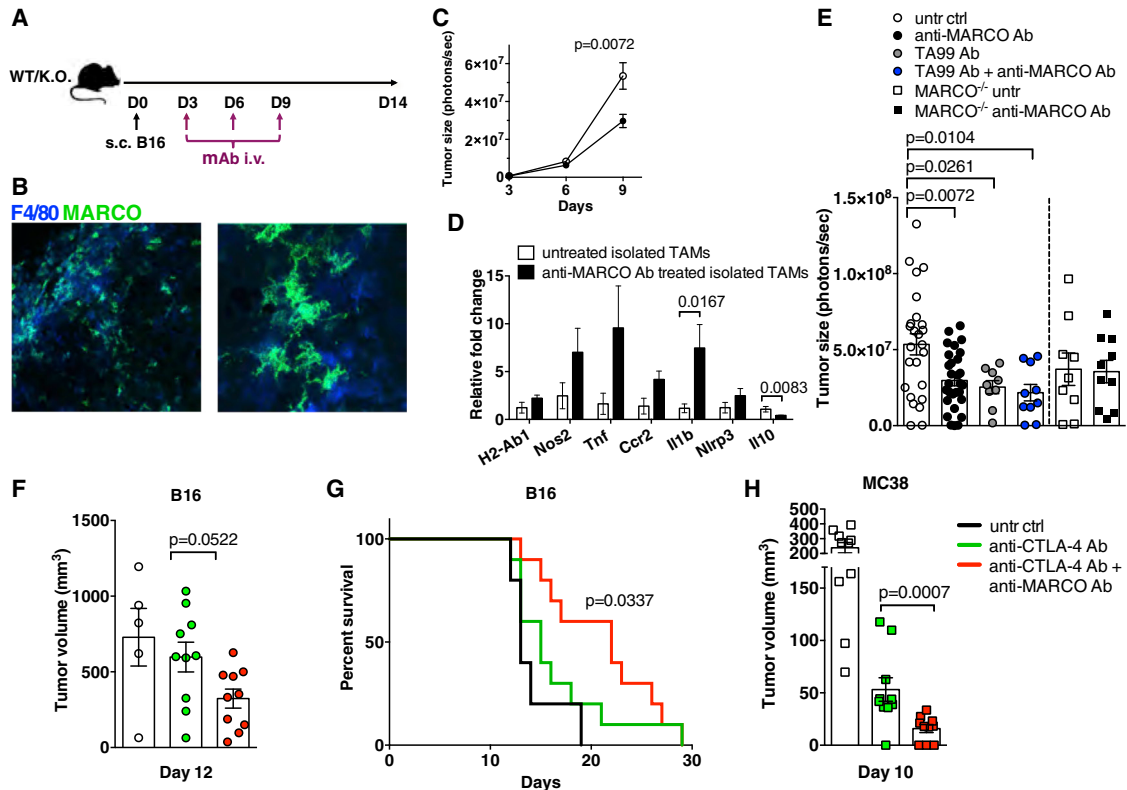


**Figure 4. Anti-MARCO Ab Treatment Inhibits Tumor Growth and Supports Immune Checkpoint Ab Therapy with Anti-CTLA-4 Ab**

(A) Schematic of the B16 melanoma tumor model and Ab treatment regimen.  
 (B) IF stainings of B16 tumors. In-vivo-administered anti-MARCO Ab (green) detected on F4/80<sup>+</sup> (blue) macrophages is shown, 63 $\times$  (left) and 100 $\times$  (right).  
 (C) B16 tumor growth curves measured by IVIS on untreated and anti-MARCO Ab-treated mice.  
 (D) M1 and M2 gene expression profile by qPCR of sorted live CD45<sup>+</sup>CD11b<sup>+</sup>Ly6G<sup>-</sup> bulk macrophages from untreated and anti-MARCO-treated B16 tumors, day 12.  
 (E) Histograms representing B16 tumor size of different combinatorial treatment groups on day 9 in wild-type (WT) and MARCO-deficient mice; n = 10–20/group.  
 (F) Histograms of B16 untreated, anti-CTLA-4 Ab+Gvax, and anti-CTLA-4 Ab+Gvax+anti-MARCO Ab-treated mice, n = 5–10/group, of two independent repeats.  
 (G) Survival analysis of mice challenged with B16 tumor cells and vaccinated on days 3, 6, and 9 with  $1 \times 10^5$  Gvax and the indicated Ab or combination i.v. Anti-MARCO treatment was continued at 3-day intervals. Lack of survival was defined as tumor volume >1,000 mm<sup>3</sup>, n = 5–10/group. Survival curves were analyzed according to Mantel-Cox log rank test; anti-CTLA-4 Ab+Gvax versus anti-CTLA-4 Ab+Gvax+ anti-MARCO Ab; p = 0.0337. In (C)–(E), data show mean  $\pm$  SEM with a CI of 95%.  
 (H) Histograms of MC38 untreated, anti-CTLA-4 Ab, and anti-CTLA-4 Ab+anti-MARCO Ab-treated mice; n = 10/group; data are representative of two independent repeats.

2001; Figures 6A and S5A). The figures show the distribution of MARCO expression stratified by breast cancer molecular subtypes. This correlates with our findings of MARCO-expressing TAMs in mice, as the 4T1 tumor model is considered to some extent to represent basal breast cancer (Kaur et al., 2012). Patients with the basal tumor subtype are also those individuals with the poorest prognosis, and the current treatment options are limited to cytotoxic agents (Badve et al., 2011). To further evaluate MARCO expression in human breast tumors, we compared it to the expression of defined immunosuppressive TAM markers (*ARG1*, *RETNLB*, *IL4R*, *CHIA*, *CD68*, and *CD163*), including Fc $\gamma$ RIIB. MARCO expression was positively correlated with all these genes except *arg1* in the The Cancer Genome Atlas (TCGA) dataset, indicating that the receptor is expressed in cancers with high M2 TAM expression signatures (Figures 6B and S5B). Next, we correlated MARCO expression

with expression of a number of EMT markers (Table S1) and observed that many of these were positively correlated with MARCO in the tumors (Figures 6C and S5C; Creighton et al., 2009). Among these genes, *mmp9* is involved in tissue remodeling and metastasis (Morini et al., 2000), and *snail* as well as *twist* are considered master regulators of EMT (Xu et al., 2009). We then used immunofluorescence staining of human breast cancer tumors to investigate MARCO expression and found it to be co-expressed on CD68<sup>+</sup> M2 TAMs as defined by CD206 and CD163 expression (Figure 6D). When quantifying MARCO<sup>+</sup> TAMs in breast cancer comparing estrogen receptor (ER)<sup>+</sup>/progesterone receptor (PR)<sup>+</sup> tumors with triple-negative (basal-like) tumors, we found that there were more TAMs in the triple-negative tumors and that the MARCO<sup>+</sup>CD163<sup>+</sup> M2 subpopulation was dominant (Figures 6E, 6F, and S5D). When investigating human metastatic melanoma, we found that MARCO was expressed

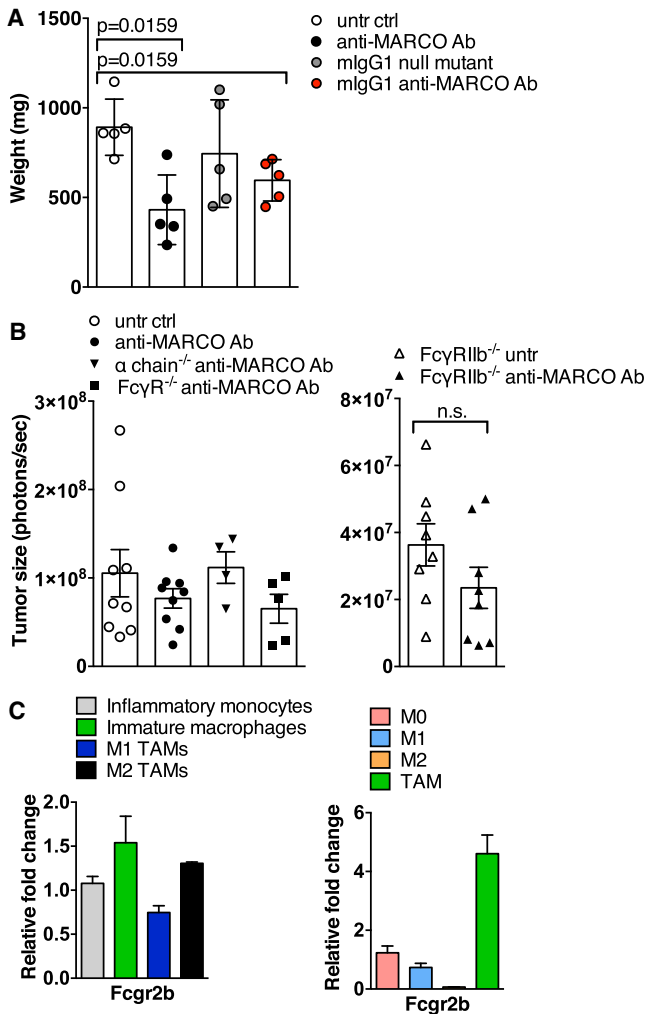


**Figure 5. The Anti-MARCO Anti-tumor Effect Is Mediated through an FcR-Dependent Mechanism**

(A) Histograms representing B16 tumor size of mice treated with Fc-modified anti-MARCO Abs compared to untreated and anti-MARCO Ab-treated mice on D10; n = 5.  
 (B) Histograms depicting B16 tumor size in FcR KO mouse strains compared to wild-type; n = 4–9/group (left) and in Fc $\gamma$ RIIb KO mice on D9; two independent experiments with n = 4/group (right).  
 (C) Relative expression of Fc $\gamma$ RIIb in tumor-infiltrating myeloid populations (Figure 1C, gates 1–4) compared to inflammatory monocytes (left) and BMDMs compared to M0 macrophages (right). Data show mean  $\pm$  SEM with a CI of 95% of duplicates.  
 In (A) and (B), data show mean  $\pm$  SEM with a CI of 95%.

more in local and distant metastases (Figure S6A). As with breast cancer, MARCO expression correlated with macrophage and M2 TAM-related genes as well as markers of EMT (Figures S6B and S6C). We also verified MARCO expression by immunofluorescence by triple staining with CD68 and the M2 marker CD163 (Figure S6D). These data suggest that anti-MARCO immunotherapy could especially benefit patients suffering from triple-negative breast cancer carcinoma and could also be effective in melanoma. Similar to the mouse models, we also found

that a subpopulation of M2 TAMs expressed MARCO and further evaluation of this subtype in other cancers is warranted.

## DISCUSSION

The success of immune checkpoint therapy has spawned an intense search for other immune-modulatory treatments for cancer, especially those that can further improve these treatments. Here, we show that using Abs that are specific for the pattern recognition receptor MARCO expressed by TAMs is a feasible way to treat mammary carcinoma, colon carcinoma, and melanoma, as well as supporting CTLA-4 treatment in two of these models. In this treatment strategy, we selectively target a specific subtype of TAMs in the tumor stroma to activate them and render the tumor immunogenic. This approach was sufficient to shift the balance of the anti-inflammatory, pro-tumorigenic, and metastatic TME to a less-supportive one for tumor progression. As a result, not only tumor growth but also metastatic spread to the lungs was inhibited. Whereas targeting TAMs has been highlighted as an attractive alternative to classic tumor treatment, the only option to date that has shown promise is cytokine blockade, a pan-macrophage approach that has limited applicability (DeNardo et al., 2011; Pyonteck et al., 2013; Strachan et al., 2013). The CSF-1 blockade has been evaluated for tumor treatment and has been tested for the ability to enhance the response to chemotherapy. The anti-MARCO treatment also enhanced an anti-tumor effect mediated by anti-CTLA4 Ab therapy in melanoma and colon carcinoma, and further studies will elucidate how it works in combination with other treatments. In melanoma, combination of checkpoint therapies have been effective, but still there are patients that are non-responders, and optimal use of T-cell-directed treatments will require combination with other therapies (Larkin et al., 2015; Twyman-Saint Victor et al., 2015). Combining these with anti-MARCO treatment would be an attractive way forward to enhance the efficacy even further without having to resort to a less-specific treatment. Mechanistically, making tumors more immunogenic by including an Ab against TAMs would increase the specific T cell response that could be further enhanced by anti-CTLA4 treatment. In addition, activating T cells to target the tumor might further polarize TAMs to a pro-inflammatory phenotype and support checkpoint therapy. The effect of anti-CTLA4 depends on the activating Fc $\gamma$ RIV expression by macrophages (Simpson et al., 2013), whereas here we find that potent anti-MARCO treatment depends on Fc $\gamma$ RIIb expression. This is similar to what has been reported for anti-CD40 treatment, which requires this receptor for immunostimulatory activity (Li and Ravetch, 2011). This Fc dependence will be an important aspect to take into consideration when designing anti-MARCO mAb therapeutics for the treatment of cancer.

We determined that MARCO expression correlated with expression of M2 markers that have been described to be expressed by tumor-promoting macrophages (Sica et al., 2008). However, macrophages are extremely plastic cells and transcriptome analyses often show mixed M1 and M2 phenotypes with several subtypes within each category (Murray et al., 2014; Qian and Pollard, 2010). We found that MARCO was expressed by a subpopulation of TAMs in the TME of both murine

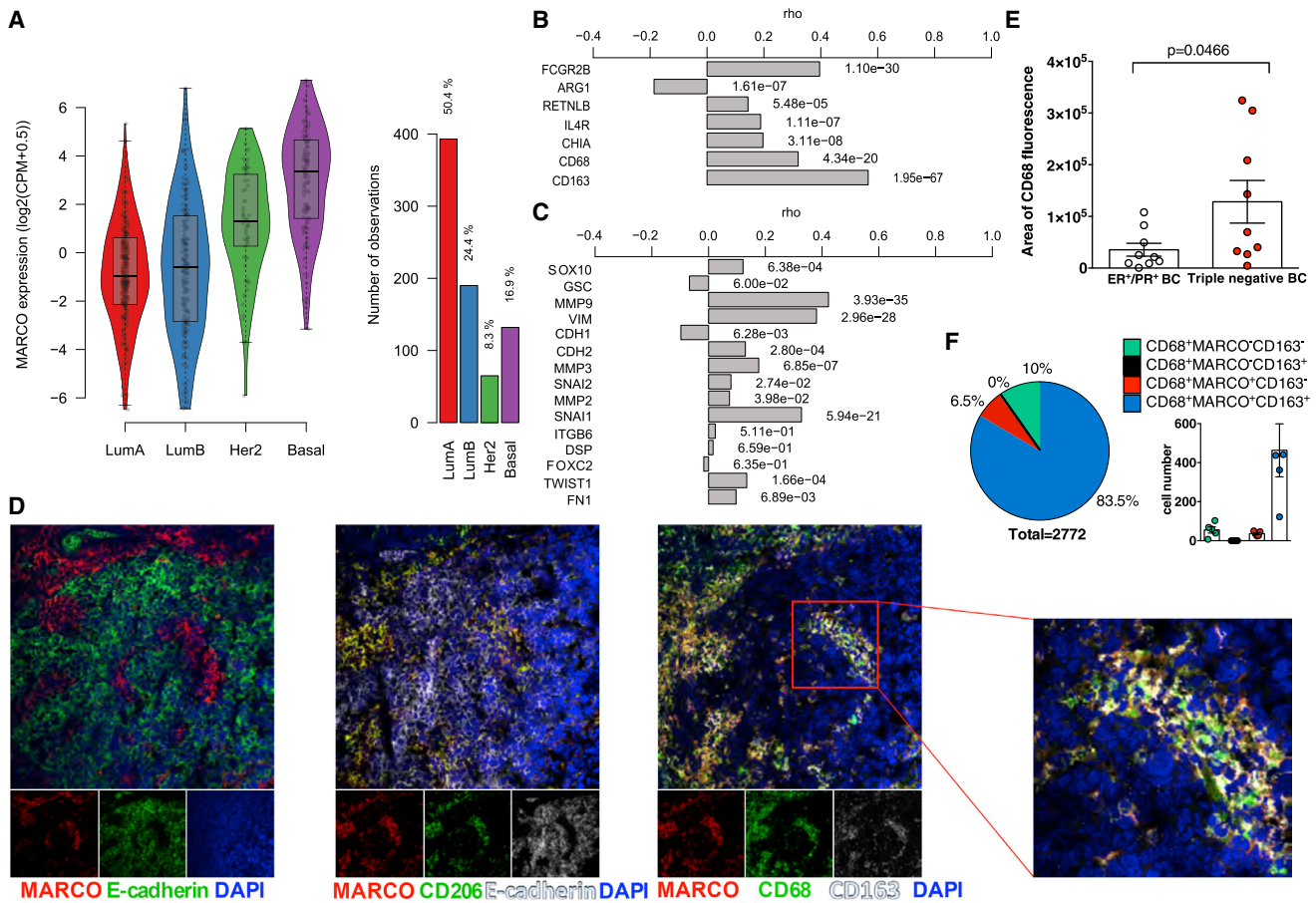


**Figure 6. MARCO Targets the Tumor Stroma of Human Triple-Negative Breast Cancer**

(A) Expression of MARCO (left panel) in human breast cancer subtypes and subtype distribution in each group (right panel) in the TCGA dataset. (B and C) Correlation of MARCO expression with the M2 gene set in the TCGA dataset (B) and with the EMT gene set in the TCGA dataset (C). (D) IF stainings of one representative human triple-negative breast cancer sample (20 $\times$ ). (Left panel) MARCO (red), tumor-marker E-cadherin (green), and DAPI (blue), in individual channels and merged, are shown. (Middle panel) MARCO (red), CD206 (green), tumor-marker E-cadherin (white), and DAPI (blue) and (right panel) MARCO (red), CD68 (green), CD163 (white), and DAPI (blue) are shown. (Far left panel) Magnification of macrophage-rich area from left panel is shown. (E) Quantification of CD68<sup>+</sup> fluorescence area in ER<sup>+</sup>/PR<sup>+</sup> and triple-negative human breast cancer sections; n = 9/group; each dot represents one sample; three non-overlapping images were obtained per sample covering the majority of the section, with the exception of one sample due to size limitations. (F) Pie chart indicating the distribution of different macrophage populations in triple-negative breast cancer samples; n = 5; three images per sample were counted, except for one sample (only one image) due to size limitation.

tumor models and in human cancer. Further characterization of the MARCO<sup>+</sup> subpopulation of TAMs is needed in other cancers to define to which extent it is clinically relevant for cancer progression. Previously, it has been shown in vitro that human monocytes can be activated to express MARCO by glucocorticoids (Gratchev et al., 2005), and here, we find that TGF- $\beta$  and IL-10 could also upregulate MARCO. This supports MARCO as a marker for potentially several subtypes of immunosuppressive TAMs. However, currently, the data available for macrophage activation are complex, and a clear translation between studies in vitro and in vivo is difficult as it is challenging to mimic all tissue or TME-related cues. In addition, activated DCs have been shown to express MARCO, and this receptor modulates their migration and efficacy in cellular immunotherapy. Thus, modulation of MARCO may also be useful beyond repolarization of TAMs.

To summarize, this study shows that reprogramming of macrophages in the TME using Abs is a feasible approach for cancer immunotherapy. These findings lead way for further screening for possible new targets on TAMs for directed Ab therapy in models where altered macrophage polarization will be beneficial. To expose the inherited immunogenicity of tumors using specific Abs has great potential and will also shed light on the function of the immune system in the context of cancer surveillance.

## EXPERIMENTAL PROCEDURES

### Cell Culture

The B16 luciferase-transfected (B16-luc) mouse melanoma cell line (kind gift from Dr. K. Weillbaecher, Washington University) and B16mOVA from Dr. Thomas Tedder (Duke University School of Medicine) was cultured in

complete medium (DMEM supplemented with 2 mM L-glutamine, 10 mM HEPES, and 10% heat-inactivated fetal calf serum [FCS]), and selective expression of the plasmid bearing the luciferase gene was maintained by addition of 100  $\mu$ g/ml Geneticin (G418) once a week during propagation. All cells used for the individual repeats of the experiment originate from the same early passage stock and are cultured for  $\sim$ 1 week before in vivo administration. The 4T1 mammary carcinoma cell line (Barbara Ann Karmanos Cancer Institute) was cultured in RPMI-1640 medium supplemented with 10% fetal bovine serum (FBS), 1% penicillin-streptomycin, and 1% glutamine. The MC38 colon adenocarcinoma cell line was cultured in RPMI-1640 medium supplemented with 10% FBS, 1% penicillin-streptomycin, and 1% glutamine. IC-21 peritoneal macrophage cell line (ATCC) was cultured in RPMI-1640 medium supplemented with 10% FBS, 1% penicillin-streptomycin, and 1% glutamine. The rat anti-MARCO IgG1 mAb hybridoma ED31 was a generous gift from Prof. G. Kraal. For generation of in vitro BMDMs, bone marrow was collected by flushing the femurs of 8- to 10-week-old C57BL/6 or MARCO KO mice with cold DMEM. After collection, red blood cells were lysed and the cells were washed twice in PBS. To induce macrophage differentiation, cells were resuspended in DMEM supplemented with 20% FCS and 20% macrophage colony-stimulating factor (M-CSF) conditioned medium collected from 3- to 4-day cultures of mouse L929 fibroblasts secreting M-CSF. The cells were plated in different-sized vessels depending on the application. On day 3, half of the volume was replaced with fresh DMEM/M-CSF, and on day 6, the entire volume was replenished. On day 10 of in vitro culture, the cells were polarized using standard conditions as reported by Mosser and Zhang (2008). More specifically, M1 classical activation was induced by addition of 20 ng/ml interferon  $\gamma$  (IFN $\gamma$ ) and 10 ng/ml lipopolysaccharide (LPS) and M2 alternative activation was induced by addition of 20 ng/ml IL-4 and 20 ng/ml IL-13; for TAMs, a supernatant from in vitro cultures of B16 was applied, and for M0, only DMEM 10% FBS was added. Alternatively, IC-21 cells and M0 BMDMs were treated with 20 ng/ml IL-10 or TGF- $\beta$  to induce MARCO upregulation. The cytokines were purchased from R&D Systems. After polarization, the cells were phenotyped, stimulated with mAbs, and used in different assays.

### Animal Studies

Mice were maintained at the Microbiology Tumor and Cell Biology Animal Facility at Karolinska Institute, and the experiments were approved by the local ethical committee (the North Stockholm district court). Wild-type C57BL/6, Balb/c (Taconic) and MARCO KO and FcR1b KO (Taconic) on C57BL/6 mixed background mice were kept and bred under pathogen-free conditions according to local ethical guidelines. FcR $\alpha$ -null (Smith et al., 2012), Fc $\gamma$ 1g $^{-/-}$  (Takai et al., 1994), humanized Fc $\gamma$ R mice (Smith et al., 2012) from J.V.R.'s laboratory at Rockefeller University were used in B16 tumor experiments and C57BL/6 for the MC38 model. Mice at the age of 8–10 weeks were injected s.c. in the right flank with  $1 \times 10^5$  (or  $2 \times 10^4$  for survival studies) B16-luc or B16mOVA cells in BD Matrigel (later taken over by Corning). At days 3, 6, and 9 of the experimental setup, mice were injected i.v. with 50 or 100  $\mu$ g of anti-MARCO mAb (rat IgG1; clone ED31), 200  $\mu$ g TA99 mAb (mouse IgG2a), and/or 100  $\mu$ g anti-CTLA-4 mAb (9D9) from Bio X cell. The anti-CTLA-4 mAb was used in combination with  $1 \times 10^6$  irradiated (150 Gy) B16-BL6 cells expressing granulocyte M-CSF (GM-CSF; GVAX) that were injected s.c. in the contralateral flank. The animals were imaged using intravital imaging (IVIS) at the same time points. For the B16 model survival studies, the tumors were measured manually every second day for the entire duration of the experiments. On day 10 of the experimental setup, the animals were sacrificed and tumors, spleens, and lymph nodes were collected for further analyses. Balb/c mice were injected in the mammary fat pad with  $2 \times 10^5$  syngeneic 4T1 mammary adenocarcinoma cells and treated with 100  $\mu$ g of anti-MARCO mAb on days 0 and 3 and thereafter with 50  $\mu$ g every third day. Mice were sacrificed on day 21, and primary tumors, lung metastases, spleens, and draining and non-draining lymph nodes were assessed. In the MC38 model,  $2 \times 10^6$  cells were injected s.c. in C57BL/6 mice. Mice were treated intraperitoneally (i.p.) with 50  $\mu$ g anti-CTLA-4 Ab on days 7, 10, and 13. Treatment with 200  $\mu$ g anti-MARCO Ab i.p. was done on days 7, 10, 13, and 17. Tumor size was monitored by manual measurements.

### Cloning and Production of Fc-Modified Variants of the Rat anti-MARCO IgG1 ED31 mAb

Cloning of the rat (anti-MARCO) IgG CDRs from ED31 hybridoma cDNA was performed using the 5' RACE system for rapid amplification of cDNA ends. A list of the primers used is presented in Table S1. Antibody expression vectors were transfected into competent *E. coli* cells and cultured to single clones that were screened for the production of the correct DNA construct. The chosen clones were expanded for plasmid purification. Plasmids were transfected into HEK293T cells for production of the different mAbs. Culture supernatants were collected, and the Abs were isolated by standard protein purification techniques using G-protein-specific separation columns.

### Lung Tumor Colony Formation Assay

Lungs were harvested in PBS + 10% FBS and dissociated in StemPro Accutase medium supplemented with TrypLE at a 1:1 ratio and 1 mg/ml Dnase in 6-well plates. They were subsequently dissected into small pieces and incubated at 37°C for 20 min. The tissue was further disturbed by passaging through a syringe (without the needle) and lastly through a syringe with a needle for further dissociation. The cell suspension was filtered through a 70- $\mu$ m cell strainer followed by treatment with erythrocyte lysis buffer. The lung cells were resuspended in RPMI-1640 medium containing 60  $\mu$ M/1 6-thioguanine (Sigma) and seeded in 10-cm plates. The culture medium was changed after 4 or 5 days. On day 10, the cells were washed and fixed in formaldehyde. After washing with distilled H<sub>2</sub>O, the cells were stained with hematoxylin for 5 min and the plates were dried upside down, after which the number of microcolonies was counted.

### Immunofluorescence

Murine tumors were cryopreserved in OCT medium NEG 50 (Thermo Scientific), and 8-mm-thick sections were cut using a cryostat microtome. After overnight drying, the slides were fixed in acetone and stored at  $-80^\circ\text{C}$ . Before staining, slides were blocked with 5% goat serum (DakoCytomation) in PBS. The following Abs were used: rat anti-MARCO produced by the ED31 hybridoma and conjugated to AF555 (Life Technologies); goat anti-rat IgG AF555 (Life Technologies); anti-F4/80 AF647/AF488; anti-CD11b AF488; anti-CD11c FITC; anti-DEC205 AF647; anti-PDCA-1 AF488; anti-TCR $\beta$  AF488; anti-CD45R AF488; anti-NK.1.1 Biotin (Biolegend); anti-CD200R AF488 (AbD serotec); and Streptavidin AF488 (Life Technologies). Slides were mounted with Prolong Diamond mounting medium. Human breast carcinoma cryosections were treated as above. After blocking with goat serum, primary Abs were incubated overnight at  $+4^\circ\text{C}$ , whereas secondary Abs were incubated for 1 hr at room temperature (RT) in 0.1% BSA PBS solution. Samples were stained with mouse-anti-human E-cadherin Ab (BD Biosciences), a rabbit-anti-human anti-MARCO Ab (Abcam), mouse-anti-human CD206 AF488 (Biolegend), and mouse-anti-human CD163 (AbDSerotec). Secondary goat-anti-mouse IgG(H+L) AF488 and goat-anti-rabbit IgG(H+L) AF555 (Life Technologies) were used for detection. Slides were mounted with DAPI-containing Prolong Diamond mounting medium. Images were collected using a confocal microscope (Leica TCS SP5 X or LSM-700; Carl Zeiss). Confocal stack images were recorded with the LSM Image software and used to generate 3D projections.

Images of three non-overlapping optical fields covering the surface of the tumor sections were captured. Image analysis was performed in ImageJ using the area measurement application, and cells were counted double blind.

### Cell Staining on Glass Coverslips or Chamber Wells

Cells were seeded in wells for overnight attachment. Prior to Ab incubation, the cells were incubated for 10 min in ice-cold DMEM, 1% BSA, and 20 mM HEPES. The cells were stained with anti-CD11b A488, anti-F4/80 A647, and anti-MARCO AF555 (ED31) for 30 min on ice in dark. The wells were washed thoroughly with 1% BSA/PBS, and the cells were fixed with 4% PFA for 20 min at RT. The cells were washed with 1% BSA/PBS and mounted with Prolong Diamond DAKO mounting medium.

### IVIS

Animals were imaged in groups of five using an IVIS Spectrum computed tomography (CT) (PerkinElmer). Mice were injected s.c. with  $1 \times 10^5$  B16-luc cells in BD Matrigel. The animals were weighed and shaved locally at the

injection site before imaging. The mice were subsequently injected i.p. with 15 mg/g body weight of the substrate D-Luciferin Potassium salt (Perkin Elmer). After determining the kinetics curve of luciferin breakdown for the B16-luc system, the optimal imaging time point was determined at around 15 min after substrate administration. As the time point of maximal bioluminescence readout fluctuated with tumor size over the course of the experiment, an imaging sequence of six segments with 5 min delay was captured per imaging session. Measurements were taken on days 3, 6, and 9, respectively, of the experimental setup. The mice were anesthetized with isoflurane for the procedure.

#### Tumor Dissociation Protocol

B16-luc tumors were harvested in cold RPMI on day 10. They were finely cut into pieces using surgical scalpels and further enzymatically dissociated through the addition of 200  $\mu$ g/ml DNase I (Roche), 200  $\mu$ g/ml hyaluronidase (Sigma), 66  $\mu$ g/ml Liberase TL (Roche), and 1 M HEPES for 30–45 min at 37°C with stirring. After 20 min of incubation, 0.1 M EDTA was added to avoid clumping. The samples were incubated for an additional 10 min on ice to allow isolation of macrophages and dendritic cells. Thereafter, the preparations were passed through a 100- $\mu$ m filter strainer and washed thoroughly with Hank's balanced salt solution (HBSS) buffer supplemented with 2% FCS, 20 mM HEPES, and 5 mM EDTA. Finally, the cells were resuspended in PBS and stained for flow cytometry. In some cases, the mouse tumor dissociation kit from Miltenyi Biotec was used, with no difference in the amount or quality of the dissociated cells. 4T1 tumors were dissociated using the Miltenyi mouse tumor dissociation kit according to the manufacturers' instructions and using the Gentle MACS dissociator (Miltenyi Biotec).

#### Flow Cytometry, Cell Sorting, and ELISA

Single-cell suspensions of tumors were prepared, and erythrocytes were lysed. Non-specific labeling was blocked with anti-CD16/32 (Fc Block; BioLegend) before specific labeling. LIVE/DEAD Aqua staining was used to remove dead cells. The cells were fixed and permeabilized (buffers from BioLegend) after surface staining. For intracellular FoxP3 staining, the manufacturer's protocol was followed (Invitrogen). All fluorescence-activated cell sorting (FACS) plots depict log<sub>10</sub> fluorescence. Cells were stained with the following rat-anti-mouse Abs from BioLegend: anti-TCR $\beta$  allophycocyanin (APC); anti-NK.1.1 PerCP-Cy5.5; anti-CD4 fluorescein isothiocyanate (FITC)/Pacific blue; anti-CD8 phycoerythrin (PE)/FITC; anti-CD45R Pacific blue/APC Cy7/FITC; anti-CD45 APC-Cy7/700; anti-CD11b PE/Cy7; anti-F4/80 APC-Cy7 and Pacific blue; anti-CD11c PerCP-Cy5.5 and PE; anti-Gr-1 Pacific blue; anti-Ly6G AF488; anti-Ly6C AF647; anti-MHCII PerCP-Cy5.5; anti-CD49d PE; anti-FoxP3 PE; anti-CD49b APC; anti-CD3-biotin; and streptavidin-Qdot605. SINFEKL-specific MHC-I pentamer biotin was used to detect CD8<sup>+</sup>-specific T cells (ProImmune). 7AAD or Live/Dead marker Aqua AmCyan (Life Technologies) was used for live-dead cell discrimination. The samples were analyzed using a BD LSR Fortessa X-20 cytometer and analyzed with FlowJo software. For sorting, after tumor dissociation, CD45<sup>+</sup> cells were positively selected from the tumor lysate by magnetic-assisted cell sorting. Live CD45<sup>+</sup> CD11b<sup>+</sup> Ly6G<sup>-</sup> cells were sorted as bulk or into the subpopulations Ly6C<sup>hi</sup> MHCII<sup>lo</sup>, Ly6C<sup>int</sup> MHCII<sup>hi</sup>, Ly6C<sup>lo</sup> MHC<sup>hi</sup>, and Ly6C<sup>lo</sup> MHCII<sup>lo</sup> subsets or live CD45<sup>+</sup>, CD11b<sup>+</sup>, Ly6G<sup>-</sup>, F4/80<sup>-</sup>, CD11c<sup>+</sup> DCs using a BD FACS Aria fusion cell sorter. For ELISA, OVA-specific IgG1, IgG2a, and IgG2b Abs from serum of tumor-bearing mice were measured by standard ELISA technique. The plates (Nunc) were coated overnight at 4°C with 10  $\mu$ g/ml of OVA and blocked with BSA for 2 hr at RT. Serum samples were diluted from 1/5 to 1/200 in blocking buffer and incubated overnight at 4°C. After washing with PBS with 0.05% Tween 20 (Sigma-Aldrich), horseradish peroxidase (HRP)-conjugated secondary anti-mouse IgG1, IgG2a, and IgG2b (Southern Biotech) were used to detect OVA-specific Abs and were incubated for 1 hr at RT. All Ab levels were expressed as optical density (OD) at 450 nm.

#### qPCR

Custom designed primers (Sigma) for qPCR were used to determine expression of a variety of macrophage polarization and cytokine genes (*h2-ab1*, *fcgr2b*, *arg1*, *marco*, *nos2*, *fizz1*, *retnl1a*, *ym1*, *chi3l3*, *il12a*, *il12b*, *cd200r*, *csf1r*, *tgfb*, *cx3cr1*, *il10*, *ccr2*, *siglec1*, *cd163*, and *rp113a* as a housekeeping gene).

In-vitro-cultured cells were lysed in RNA later (RLT) buffer with 1%  $\beta$ -mercaptoethanol (Life Technologies), and RNA preparation was performed using the QIAGEN Rneasy micro/mini plus kit. cDNA was synthesized using iScript (Bio-Rad) under standard conditions. qPCR using SYBRGreen (Bio-Rad) was performed on a CFX96 real-time cycler (Bio-Rad) and analyzed according to the Livak method for relative expression.

#### Human Breast Cancer and Melanoma Samples

Tumor tissue from women (n = 18) operated for invasive breast cancer were collected at Department of Surgery, Umea University. Samples were collected during surgery, snap frozen in liquid nitrogen, and kept at -80°C until analysis. Five-micrometer sections were cut and used for immunofluorescence analysis as described above. The cohort consisted of ten women with ER- and PR-positive and ten women with ER- and PR-negative disease, respectively. Eight out of 20 women had axillary lymph node metastasis at the time of surgery. In regards to molecular subtypes of breast cancer, the cohort consisted of seven Luminal A, one Luminal B, five Her-2-amplified, and seven triple-negative breast cancer patients. Informed consent was obtained from all patients. Ethical approval was obtained from the ethical committee (EPN) of Northern Sweden. For melanoma, metastases from patients with cutaneous melanoma, who underwent surgery at the Karolinska University Hospital, were included in this study. The specimens were fresh frozen in liquid nitrogen and kept in a bio-bank until analysis. Biobanking and analysis of patient samples was approved by the Stockholm Regional Ethics Committee.

#### Statistics

Data were analyzed by unpaired Student's t test or Mann-Whitney U t test to compare two groups. A p value of <0.05% was considered to be statistically significant. Survival was analyzed with the log rank (Mantel-Cox) test.

#### RNA-Seq Data Processing and Analysis

##### TCGA Breast Cancer Dataset

Clinical data from the TCGA invasive breast carcinoma dataset (provisional) were downloaded from the TCGA data portal (<https://tcga-data.nci.nih.gov/tcga/>) on 11<sup>th</sup> of December 2013 and included data for 1,148 cases. Unaligned RNA-seq data from the TCGA dataset were subsequently downloaded (June 2014) after approval from the TCGA data access committee (n = 1,126; all available cases with unaligned data). A total of 1,073 cases were available with both unaligned RNA-seq data and clinical data. Of these, 35 observations were excluded as potential outliers based on inspection of principal-component analysis scores and residuals. A total of 885 of the 1,038 cases had molecular subtype (PAM50) assignments available. All remaining cases classified as normal-like subtype (n = 105) were excluded, as the clinical relevance for this subtype has been questioned (Eroles et al., 2012), leaving 780 samples for further analysis.

##### Tissue Collection, RNA Extraction, RNA Library Construction, and Sequencing for the ClinSeq Breast Cancer Dataset

Tumor tissues from 255 patients diagnosed with breast cancer between 2006 and 2010 at the Karolinska Hospital and 63 patients during 2012 at South General Hospital in Stockholm were snap-frozen on dry ice and stored at -80°C. The ClinSeq breast cancer study has approval from the Regional Ethical Review Board in Stockholm. RNA was extracted from fresh frozen tumors using AllPrep DNA/RNA/Protein mini kit (QIAGEN). RNA was assessed using bioanalyzer to ensure high quality (RNA integrity number [RIN] > 8). One microgram of total RNA was used for rRNA depletion using RiboZero (Illumina), and stranded RNA-seq libraries were constructed using a TruSeq Stranded Total RNA Library Prep Kit (Illumina). Sequencing was performed using an Illumina HiSeq 2500 at Science for Life Laboratories. In total, the ClinSeq dataset contained 318 cases with RNA-seq data. Of these, 11 were excluded as potential outliers based on inspection of principal-component scores and residuals, leaving 307 samples for analyses.

##### Bioinformatic Pre-processing of RNA-Seq Data

Standard Illumina adapters (AGATCGGAAGAGCACACGTCTGAACTCCAGT CAC and AGATCGGAAGAGCGTCGTGTAGGGAAAGAGTGTGA) were trimmed using skewer version 0.1.117 (Jiang et al., 2014) with default parameters for both single-end and paired-end data. Alignment was conducted using STAR aligner version 2.4.0e (Dobin et al., 2013) with the following parameters: "-outSAMmapqUnique 50," to set the mapping quality of uniquely mapped

reads to 50; “-outSAMUnmapped Within,” to include unmapped reads in the resulting SAM file; “-chimSegmentMin 20” to require that a minimum of 20 bases maps to each end of a chimeric transcript (output in a separate file); and “-outSAMattributes NH HI AS nM NM MD XS,” to include additional attributes in the SAM file. Gene expression estimates were calculated with HTSeq count version 0.6.0 (Anders et al., 2015) with the following parameters: “-stranded=no” for TCGA, because the TCGA Breast Cancer RNA-seq data are non-stranded or “-stranded=reverse” for ClinSeq data and “-mode = intersection-nonempty” for counting reads. The RNA-seq count data were normalized using the TMM method (Robinson and Oshlack, 2010) provided in the edgeR package (Robinson et al., 2010). Gene expression values are expressed as  $\log_2$  (counts per million), abbreviated as  $\log_2$  (CPM). Molecular subtypes of tumors in the ClinSeq dataset were assigned by applying the method described by Parker et al. (2009) and using the TCGA dataset to estimate model parameters. To account for potential batch differences, the two datasets were pre-processed using the same bioinformatic pipeline and variables were mean-centered and scaled to unit variance. Marginal correlation between MARCO and genes in the “M2 gene set” and the “EMT gene set” was assessed by means of Spearman’s rank correlation coefficient ( $\rho$ ) with p values based on a two-sided test, using the *cor.test* function in R, with p values calculated using the function *pSpearman()* in the R package “SuppDists”. RNA-seq gene expression data (RNaseq v2 [level 3]; quantified by RNA-seq by expectation maximization (RSEM); Li and Dewey, 2011) from 469 Skin Cutaneous Melanoma patients were downloaded from TCGA data portal together with clinical data. RNA-seq data were normalized using the same method as described above. Samples with “submitted tumor site” annotated as “distant metastasis” (n = 68), “primary tumor” (n = 102), “local cutaneous or subcutaneous tissue” (includes satellite and in-transit metastasis) (n = 74), or “local lymph node” (n = 222) were used in subsequent analyses (466 tumors in total).

## SUPPLEMENTAL INFORMATION

Supplemental Information includes six figures and two tables and can be found with this article online at <http://dx.doi.org/10.1016/j.celrep.2016.04.084>.

## AUTHOR CONTRIBUTIONS

A.-M.G., J.V.R., and M.C.I.K. designed experiments, analyzed data, and wrote the manuscript. A.-M.G., K.P., E.H., V.F.B., J.Ö., R.D., and S.S. performed experiments. R.A.H., C.R., J.F., S.E.B., and F.L. provided technical expertise. M.R. and D.K. analyzed data in the clinical studies. M.S. and S.E.B. provided biopsies of clinical material.

## ACKNOWLEDGMENTS

M.C.I.K. was supported by the Swedish Cancer Foundation. J.V.R. was supported by the Rockefeller University. J.F. was supported by the Swedish Cancer Foundation, the Swedish Research Council, the Strategic Cancer Programme at Karolinska Institutet, and the Nordic Cancer Union. The ClinSeq project was supported by the Strategic Cancer Programme (Stratcan) at Karolinska Institutet and the Swedish Research Council. M.R. was supported by Karolinska Institutet and the Swedish Research Council. We thank Ralph Steinman and Siamon Gordon for discussions on the role of MARCO in cancer and important technical insight and Lotta Von Boehmer for critically reading the manuscript. We thank Katherine Weibaecher for the B16luc cell line; Thomas Tedder for the B16mOVA cell line; George Kraal for the ED31 hybridoma; and Karl Tryggvasson, Timo Pikkarainen, and Juha Ojala for the MARCO knockout mice and scavenger receptor expertise. We also thank Rolf Kiessling and Johan Hansson for assistance with melanoma samples and Malin Wine-rdahl for illustrations. In addition, we thank Patrick Smith, Emma Lindh, Annette Berglund, and Saikiran Sedimbi for technical assistance.

Received: June 10, 2015  
Revised: March 2, 2016  
Accepted: April 21, 2016  
Published: May 19, 2016

## REFERENCES

- Anders, S., Pyl, P.T., and Huber, W. (2015). HTSeq—a Python framework to work with high-throughput sequencing data. *Bioinformatics* 31, 166–169.
- Badve, S., Dabbs, D.J., Schnitt, S.J., Baehner, F.L., Decker, T., Eusebi, V., Fox, S.B., Ichihara, S., Jacquemier, J., Lakhani, S.R., et al. (2011). Basal-like and triple-negative breast cancers: a critical review with an emphasis on the implications for pathologists and oncologists. *Mod. Pathol.* 24, 157–167.
- Bergamaschi, A., Tagliabue, E., Sørlie, T., Naume, B., Triulzi, T., Orlandi, R., Russnes, H.G., Nesland, J.M., Tammi, R., Auvinen, P., et al. (2008). Extracellular matrix signature identifies breast cancer subgroups with different clinical outcome. *J. Pathol.* 214, 357–367.
- Clynes, R., Takechi, Y., Moroi, Y., Houghton, A., and Ravetch, J.V. (1998). Fc receptors are required in passive and active immunity to melanoma. *Proc. Natl. Acad. Sci. USA* 95, 652–656.
- Clynes, R.A., Towers, T.L., Presta, L.G., and Ravetch, J.V. (2000). Inhibitory Fc receptors modulate in vivo cytotoxicity against tumor targets. *Nat. Med.* 6, 443–446.
- Creighton, C.J., Li, X., Landis, M., Dixon, J.M., Neumeister, V.M., Sjolund, A., Rimm, D.L., Wong, H., Rodriguez, A., Herschkowitz, J.I., et al. (2009). Residual breast cancers after conventional therapy display mesenchymal as well as tumor-initiating features. *Proc. Natl. Acad. Sci. USA* 106, 13820–13825.
- DeNardo, D.G., Brennan, D.J., Rexhepaj, E., Ruffell, B., Shiao, S.L., Madden, S.F., Gallagher, W.M., Wadhvani, N., Keil, S.D., Junaid, S.A., et al. (2011). Leukocyte complexity predicts breast cancer survival and functionally regulates response to chemotherapy. *Cancer Discov.* 1, 54–67.
- Dobin, A., Davis, C.A., Schlesinger, F., Drenkow, J., Zaleski, C., Jha, S., Batut, P., Chaisson, M., and Gingeras, T.R. (2013). STAR: ultrafast universal RNA-seq aligner. *Bioinformatics* 29, 15–21.
- Dougan, M., and Dranoff, G. (2009). Immune therapy for cancer. *Annu. Rev. Immunol.* 27, 83–117.
- Elomaa, O., Kangas, M., Sahlberg, C., Tuukkanen, J., Sormunen, R., Liakka, A., Thesleff, I., Kraal, G., and Tryggvason, K. (1995). Cloning of a novel bacteria-binding receptor structurally related to scavenger receptors and expressed in a subset of macrophages. *Cell* 80, 603–609.
- Eroles, P., Bosch, A., Pérez-Fidalgo, J.A., and Lluch, A. (2012). Molecular biology in breast cancer: intrinsic subtypes and signaling pathways. *Cancer Treat. Rev.* 38, 698–707.
- Franklin, R.A., Liao, W., Sarkar, A., Kim, M.V., Bivona, M.R., Liu, K., Pamer, E.G., and Li, M.O. (2014). The cellular and molecular origin of tumor-associated macrophages. *Science* 344, 921–925.
- Fuxe, J., and Karlsson, M.C. (2012). TGF- $\beta$ -induced epithelial-mesenchymal transition: a link between cancer and inflammation. *Semin. Cancer Biol.* 22, 455–461.
- Gratchev, A., Kzhyshkowska, J., Utikal, J., and Goerdt, S. (2005). Interleukin-4 and dexamethasone counterregulate extracellular matrix remodelling and phagocytosis in type-2 macrophages. *Scand. J. Immunol.* 61, 10–17.
- Jiang, H., Lei, R., Ding, S.W., and Zhu, S. (2014). Skewer: a fast and accurate adapter trimmer for next-generation sequencing paired-end reads. *BMC Bioinformatics* 15, 182.
- Kaur, P., Nagaraja, G.M., Zheng, H., Gizachew, D., Galukande, M., Krishnan, S., and Asea, A. (2012). A mouse model for triple-negative breast cancer tumor-initiating cells (TNBC-TICs) exhibits similar aggressive phenotype to the human disease. *BMC Cancer* 12, 120.
- Larkin, J., Chiarion-Sileni, V., Gonzalez, R., Grob, J.J., Cowey, C.L., Lao, C.D., Schadendorf, D., Dummer, R., Smylie, M., Rutkowski, P., et al. (2015). Combined nivolumab and ipilimumab or monotherapy in untreated melanoma. *N. Engl. J. Med.* 373, 23–34.
- Leach, D.R., Krummel, M.F., and Allison, J.P. (1996). Enhancement of anti-tumor immunity by CTLA-4 blockade. *Science* 271, 1734–1736.
- Li, B., and Dewey, C.N. (2011). RSEM: accurate transcript quantification from RNA-Seq data with or without a reference genome. *BMC Bioinformatics* 12, 323.

- Li, F., and Ravetch, J.V. (2011). Inhibitory Fc $\gamma$  receptor engagement drives adjuvant and anti-tumor activities of agonistic CD40 antibodies. *Science* 333, 1030–1034.
- Mani, S.A., Guo, W., Liao, M.J., Eaton, E.N., Ayyanan, A., Zhou, A.Y., Brooks, M., Reinhard, F., Zhang, C.C., Shipitsin, M., et al. (2008). The epithelial-mesenchymal transition generates cells with properties of stem cells. *Cell* 133, 704–715.
- Matsushita, N., Komine, H., Grolleau-Julius, A., Pilon-Thomas, S., and Mulé, J.J. (2010). Targeting MARCO can lead to enhanced dendritic cell motility and anti-melanoma activity. *Cancer Immunol. Immunother.* 59, 875–884.
- Miettinen, P.J., Ebner, R., Lopez, A.R., and Derynck, R. (1994). TGF- $\beta$  induced transdifferentiation of mammary epithelial cells to mesenchymal cells: involvement of type I receptors. *J. Cell Biol.* 127, 2021–2036.
- Morini, M., Mottolese, M., Ferrari, N., Ghorzo, F., Buglioni, S., Mortarini, R., Noonan, D.M., Natali, P.G., and Albin, A. (2000). The alpha 3 beta 1 integrin is associated with mammary carcinoma cell metastasis, invasion, and gelatinase B (MMP-9) activity. *Int. J. Cancer* 87, 336–342.
- Mosser, D.M., and Edwards, J.P. (2008). Exploring the full spectrum of macrophage activation. *Nat. Rev. Immunol.* 8, 958–969.
- Mosser, D.M., and Zhang, X. (2008). Activation of murine macrophages. *Curr. Protoc. Immunol. Chapter 14*, Unit 14.2.
- Movahedi, K., Laoui, D., Gysemans, C., Baeten, M., Stangé, G., Van den Bossche, J., Mack, M., Pipeleers, D., In't Veld, P., De Baetselier, P., and Van Ginnechten, J.A. (2010). Different tumor microenvironments contain functionally distinct subsets of macrophages derived from Ly6C(high) monocytes. *Cancer Res.* 70, 5728–5739.
- Murray, P.J., Allen, J.E., Biswas, S.K., Fisher, E.A., Gilroy, D.W., Goerdt, S., Gordon, S., Hamilton, J.A., Ivashkiv, L.B., Lawrence, T., et al. (2014). Macrophage activation and polarization: nomenclature and experimental guidelines. *Immunity* 41, 14–20.
- Noy, R., and Pollard, J.W. (2014). Tumor-associated macrophages: from mechanisms to therapy. *Immunity* 41, 49–61.
- Parker, J.S., Mullins, M., Cheang, M.C., Leung, S., Voduc, D., Vickery, T., Davies, S., Fauron, C., He, X., Hu, Z., et al. (2009). Supervised risk predictor of breast cancer based on intrinsic subtypes. *J. Clin. Oncol.* 27, 1160–1167.
- Pyonteck, S.M., Akkari, L., Schuhmacher, A.J., Bowman, R.L., Sevenich, L., Quail, D.F., Olson, O.C., Quick, M.L., Huse, J.T., Teijeiro, V., et al. (2013). CSF-1R inhibition alters macrophage polarization and blocks glioma progression. *Nat. Med.* 19, 1264–1272.
- Qian, B.Z., and Pollard, J.W. (2010). Macrophage diversity enhances tumor progression and metastasis. *Cell* 141, 39–51.
- Robinson, M.D., and Oshlack, A. (2010). A scaling normalization method for differential expression analysis of RNA-seq data. *Genome Biol.* 11, R25.
- Robinson, M.D., McCarthy, D.J., and Smyth, G.K. (2010). edgeR: a Bioconductor package for differential expression analysis of digital gene expression data. *Bioinformatics* 26, 139–140.
- Sharma, P., and Allison, J.P. (2015). The future of immune checkpoint therapy. *Science* 348, 56–61.
- Sica, A., Larghi, P., Mancino, A., Rubino, L., Porta, C., Totaro, M.G., Rimoldi, M., Biswas, S.K., Allavena, P., and Mantovani, A. (2008). Macrophage polarization in tumour progression. *Semin. Cancer Biol.* 18, 349–355.
- Simpson, T.R., Li, F., Montalvo-Ortiz, W., Sepulveda, M.A., Bergerhoff, K., Arce, F., Roddie, C., Henry, J.Y., Yagita, H., Wolchok, J.D., et al. (2013). Fc-dependent depletion of tumor-infiltrating regulatory T cells co-defines the efficacy of anti-CTLA-4 therapy against melanoma. *J. Exp. Med.* 210, 1695–1710.
- Sinha, P., Clements, V.K., Fulton, A.M., and Ostrand-Rosenberg, S. (2007). Prostaglandin E2 promotes tumor progression by inducing myeloid-derived suppressor cells. *Cancer Res.* 67, 4507–4513.
- Smith, P., DiLillo, D.J., Bournazos, S., Li, F., and Ravetch, J.V. (2012). Mouse model recapitulating human Fc $\gamma$  receptor structural and functional diversity. *Proc. Natl. Acad. Sci. USA* 109, 6181–6186.
- Solito, S., Marigo, I., Pinton, L., Damuzzo, V., Mandruzzato, S., and Bronte, V. (2014). Myeloid-derived suppressor cell heterogeneity in human cancers. *Ann. N Y Acad. Sci.* 1319, 47–65.
- Sørlie, T., Perou, C.M., Tibshirani, R., Aas, T., Geisler, S., Johnsen, H., Hastie, T., Eisen, M.B., van de Rijn, M., Jeffrey, S.S., et al. (2001). Gene expression patterns of breast carcinomas distinguish tumor subclasses with clinical implications. *Proc. Natl. Acad. Sci. USA* 98, 10869–10874.
- Strachan, D.C., Ruffell, B., Oei, Y., Bissell, M.J., Coussens, L.M., Pryer, N., and Daniel, D. (2013). CSF1R inhibition delays cervical and mammary tumor growth in murine models by attenuating the turnover of tumor-associated macrophages and enhancing infiltration by CD8(+) T cells. *Oncolimmunology* 2, e26968.
- Takai, T., Li, M., Sylvestre, D., Clynes, R., and Ravetch, J.V. (1994). FcR gamma chain deletion results in pleiotropic effector cell defects. *Cell* 76, 519–529.
- Taylor, R.P., and Lindorfer, M.A. (2008). Immunotherapeutic mechanisms of anti-CD20 monoclonal antibodies. *Curr. Opin. Immunol.* 20, 444–449.
- Thomson, T.M., Mattes, M.J., Roux, L., Old, L.J., and Lloyd, K.O. (1985). Pigmentation-associated glycoprotein of human melanomas and melanocytes: definition with a mouse monoclonal antibody. *J. Invest. Dermatol.* 85, 169–174.
- Twyman-Saint Victor, C., Rech, A.J., Maity, A., Rengan, R., Pauken, K.E., Stelekati, E., Benci, J.L., Xu, B., Dada, H., Odorizzi, P.M., et al. (2015). Radiation and dual checkpoint blockade activate non-redundant immune mechanisms in cancer. *Nature* 520, 373–377.
- Xu, J., Lamouille, S., and Derynck, R. (2009). TGF- $\beta$ -induced epithelial to mesenchymal transition. *Cell Res.* 19, 156–172.